An Exciton-Coupled Circular Dichroism Protocol for the Determination of Identity, Chirality, and Enantiomeric Excess of Chiral Secondary Alcohols

ARTICLE *in* JOURNAL OF THE AMERICAN CHEMICAL SOCIETY · MARCH 2012

Impact Factor: 12.11 · DOI: 10.1021/ja301252h · Source: PubMed

JACS
JOURNAL OF THE AMERICAN CHEMICAL SOCIETY

Article

pubs.acs.org/JACS

An Exciton-Coupled Circular Dichroism Protocol for the Determination of Identity, Chirality, and Enantiomeric Excess of Chiral Secondary Alcohols

Lei You,[†] Gennaro Pescitelli,[‡] Eric V. Anslyn,*[,†] and Lorenzo Di Bari*[,‡]

[†]Department of Chemistry and Biochemistry, The University of Texas at Austin, Austin, Texas 78712, United States
[‡]Dipartimento di Chimica e Chimica Industriale, Università di Pisa, Via Risorgimento 35, I-56126 Pisa, Italy

Supporting Information

ABSTRACT: Chiral mono-ols are among the most sought after targets in asymmetric synthesis, and therefore, their chemical characterization and associated enantiomeric excess (*ee*) values are commonly reported. A simple optical method for determining alcohol identity and *ee* could be widely used. Toward this end, an in situ-generated multicomponent assembly that creates diastereomeric tris(pyridine) metal complexes incorporating chiral secondary alcohols was explored using exciton-coupled circular dichroism (ECCD). Qualitative models were proposed to predict the preferential diastereomer and its twist, and computational studies provided a rationalization of the CD spectra. Different ECCD spectra found for diastereomers formed in the self-assembled tris(pyridine) complexes were used to determine the absolute configurations of chiral mono-ols. Linear discriminant analysis was successfully employed to classify the alcohol analytes, thereby allowing identification of the alcohols. Conformational effects imparted by heteroatoms were also explored, further expanding the substrate scope. Finally, *ee* calibration curves allowed the determination of the *ee* of unknown samples of three chiral secondary alcohols with an average error of 3%. The assay described here is unique because no preparation of structurally elaborated chiral hosts is needed.

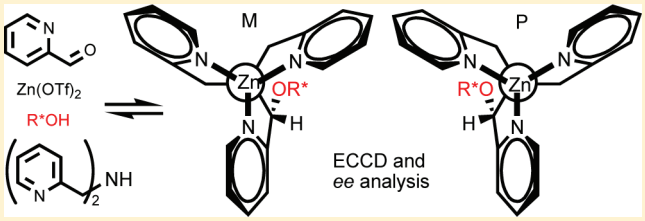

INTRODUCTION

Stereoselective synthesis is a major research area in organic chemistry, and numerous asymmetric reactions based upon either metal catalysis or organocatalysis have been developed for the preparation of chiral secondary alcohols.[1−5] Such alcohols are one of the most common functional groups found in natural products and pharmaceuticals, as well as synthetic intermediates. Because of the development of technologies for parallel synthesis and screening for catalyst optimization purposes, there is a need for rapid analysis of the absolute configuration and enantiomeric excess (*ee*) of the products of asymmetric reactions,[6,7] such as chiral secondary alcohols.

The traditional chromatographic techniques of GC and HPLC are not as readily adaptable to high-throughput screening (HTS) of *ee* as optical methods could be,[8,9] and as a result, the analysis of chirality by various spectroscopic methods is currently of interest.[10] Optical methods are fast and cost-effective and, importantly, can be easily implemented into HTS. Our group and others have pioneered the development of enantioselective indicator displacement assays (eIDAs) using colorimetric indicators.[11−13] Various colorimetric or fluorescent chiral hosts have also been explored for the purpose of chirality sensing.[14,15] Furthermore, we have used circular dichroism (CD)-active metal-to-ligand charge transfer (MLCT) bands for the determination of *ee*.[16−18] However, no group has yet created a colorimetric, fluorescent, or MLCT-CD method for the analysis of chiral secondary monoalcohols.

Exciton-coupled circular dichroism (ECCD) has often been employed for nonempirical assignment of the absolute configuration of organic molecules.[19−22] It results from the coupling of the excited states of at least two asymmetrically oriented and proximal chromophores. ECCD-based receptors have been investigated for the assignment of the absolute configurations of chiral amines[23−25] and hydroxyl-containing bifunctional substrates, including 1,2-aminoalcohols,[26] vicinal diols,[27] and epoxy alcohols.[28] Simple chiral mono-ols, however, generally need to be derivatized via chemical synthesis and purification to enhance their binding to a host that would yield a CD signal.[29−31] For other functional groups, Canary has studied the ECCD properties of chiral tripodal ligand-based complex **1**,[32] which shows *M* and *P* helical chirality[33−36] as a function of amino acid handedness. A collaborative study between our two groups elucidated an ECCD-based sensing method for the discrimination of chiral carboxylates using the achiral tripodal ligand in complex **2**.[37]

On the basis of the precedent of structures **1** and **2**, we reasoned that if a chiral alkoxy group could be placed at the benzylic position within analogous complexes, a hemiaminal

Received: February 9, 2012
Published: March 22, 2012

   dx.doi.org/10.1021/ja301252h | *J. Am. Chem. Soc.* 2012, 134, 7117−7125

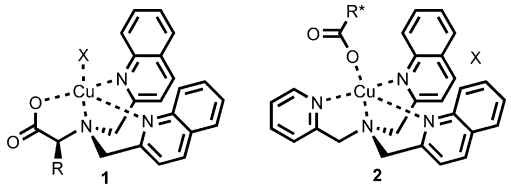

ether that in principle would give similar ECCD signals would be generated. To achieve this design concept, we created a multicomponent assembly of pyridine-2-carboxaldehyde (**2-PA**), di(2-picolyl)amine (**DPA**), zinc triflate, and a mono-ol that affords complexes such as **3** in the presence of molecular sieves and 4-(2-chloroethyl)morpholine hydrochloride (CEM-HCl) as a catalyst (Scheme 1).[38] This assembly was found to

Scheme 1. Multicomponent Assembly for the Reversible Covalent Binding of Chiral Secondary Alcohols To Give the Assembled Complex 3 Used as a Sensing Ensemble in This Study (X Represents Counterions for the Metal Center)

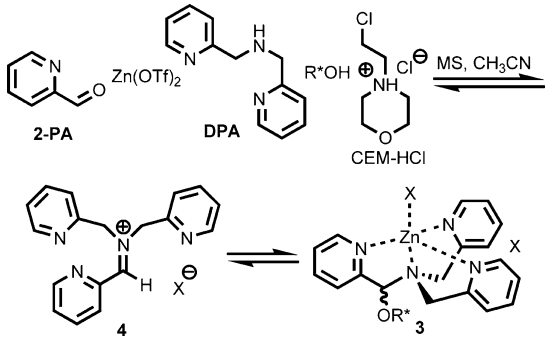

exchange aldehydes as well as alcohols reversibly.[38] The multicomponent reaction was found to be general, and an iminium ion (**4**) was supported as an intermediate. We also demonstrated the potential of this system for chirality sensing using a model alcohol.

In the current work, we explored in detail the origin of ECCD induced by chiral secondary alcohols as well as the scope of alcohol analytes that can be used for chirality sensing and *ee* measurements. Our goal was to demonstrate the generality of our multicomponent-assembly-based assay. We present a model that predicts the preferential diastereomer and the associated dominant helical twist by analysis of X-ray structural data and molecular modeling. Furthermore, computational studies creating simulated CD data are compared to the experimental spectra as a means of illustrating the structural basis of the ECCD. In addition to classification of alcohol handedness, discrimination of alcohol identity was achieved using pattern recognition protocols. The effect of the alcohol conformation on the CD signal was also investigated. Lastly, *ee* analysis using representative alcohols is presented.

RESULTS AND DISCUSSION

Diastereoselectivity. Six chiral alcohols were chosen for this study to span a range of chemical space of the R groups on the stereocenter (Scheme 2), representing linear alkyl [2-butanol (**BUO**) and 2-octanol (**OCO**)], branched alkyl [3-methyl-2-butanol (**MBO**)], aromatic [1-phenylethanol (**PEO**)], and aliphatic cyclic [*trans*-2-phenylcyclohexanol (**PCO**) and dihydrocarveol (**DHO**)]. The multicomponent assembly reaction was conducted with each chiral alcohol in the

Scheme 2. Structure of the Chiral Secondary Alcohols Studied (Only *R* Stereochemistry Is Shown)

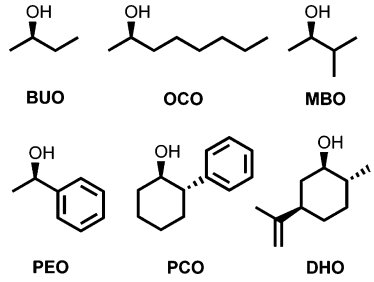

presence of activated 3 Å molecular sieves. Electrospray ionization mass spectrometry (ESI-MS) and ^{1}H NMR spectroscopy confirmed the assembly with each alcohol (yields near or greater than 80% at equilibrium). The successful binding of the sterically hindered **PCO** demonstrates the power of our in situ derivatization strategy.

Because the faces of the iminium ion intermediate **4** are enantiotopic,[39] the addition of a chiral alcohol leads to a pair of diastereomers. The resulting diastereomeric ratios (*dr*, defined as the concentration ratio of the major diastereomer over the minor diastereomer) at equilibrium were measured by ^{1}H NMR spectroscopy via integration of the methine hydrogens on the newly formed stereocenter in complex **3** as well as the hydrogens of the chiral alcohol (see the Supporting Information). Pure enantiomers of each chiral alcohol afford equal but opposite diastereoselectivity, as required by the principles of stereochemistry, and hence, the *dr* values for two enantiomeric alcohols are the same. As a result, the *dr* value is independent of the enantiomeric purity of the chiral alcohol. For **PEO** and **PCO**, the *dr* values are >2, while for **BUO** and **OCO**, the ratios are more modest (1.2−1.3). The other alcohols have *dr* values between these extremes. The *dr* value for the **DHO**-derived assembly was not obtained because of coincidental overlap of the NMR signals.

Stereoisomers. For alcohols that are not enantiomerically pure, four diastereomers are created in the assembly on the basis of two stereocenters (Scheme 3). Each of these four complexes can have a clockwise (*M*) or counterclockwise (*P*) twist of the pyridine ligands, thus resulting in a further pair of diastereomers for each, giving eight diastereomers overall. However, the *M* and *P* twists of the pyridines were anticipated

Scheme 3. Stereoisomers of Complex 3[a]

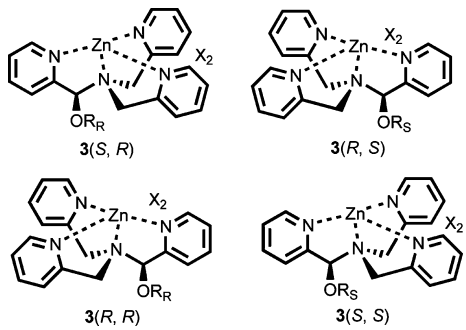

[a]The enantiomers are placed as mirror images. The first letter in the parentheses indicates the handedness of the newly formed stereocenter (i.e., the hemiaminal ether carbon), while the second represents the chirality of the stereocenter at the α-carbon of the alcohol.

dx.doi.org/10.1021/ja301252h | J. Am. Chem. Soc. 2012, 134, 7117−7125

to interchange rapidly, although one should dominate. We anticipated that the dominant twist would be dictated by the handedness of the newly formed stereocenter at the hemiaminal ether carbon. Furthermore, the diastereoselectivity should be influenced by the structure and geometry of the chiral secondary alcohol used in the assembly. For alcohol analytes that are not enantiomerically pure, all of the isomers of **3** contribute to the overall CD signal. One key feature of the assembly is that all of the diastereomers come to equilibrium because the system is dynamic. Therefore, the creation of simple chemical models of steric interactions that explain the diastereoselectivity and pyridine helical twists should lead to methods for predicting the CD spectra.

Helical Twist. To start the process of tying the ultimate CD signal to the chirality and identity of the chiral secondary alcohol, we first analyzed crystal structures in order to predict the most favorable helical twist of diastereomers of **3**. Canary reported complex **5** based on a chiral tripodal ligand that has an *R* stereocenter at the benzylic position. An X-ray crystal structure of this complex shows an *M* twist.[33] Moreover, the similar crystal structure of racemic complex **6** reported by Canary shows *M* and *P* propeller twists for the *R* and *S* isomers, respectively.[40]

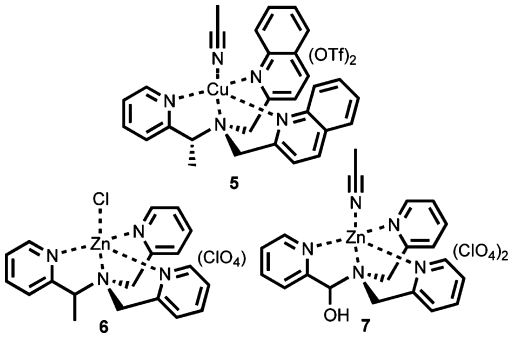

We obtained a crystal structure of racemic hemiaminal complex **7**.[41] Both *R*-**7** and *S*-**7** are present in the unit cell of the crystal structure, with zinc adopting a trigonal-bipyramidal geometry (Figure 1). A solvent molecule, acetonitrile, is bound to zinc at the axial position. The crystal structures are shown looking down the axis of acetonitrile to the zinc center and then to the tertiary amine nitrogen (hydrogens have been omitted for clarity) with the associated Newman projections placed beside them for comparison. A tilting of the three pyridine rings with respect to the $CH_3CN-Zn-N$ axis was apparent for both *R*-**7** (Figure 1a) and *S*-**7** (Figure 1b), with *M* and *P* twists, respectively. From the structural analyses of **5**, **6**, and **7**, it is evident that the same direction of helical twist depending upon the stereocenter configuration was found in all cases.

The difference between **3**, **6**, and **7** is the substituent at the benzylic position (the alkoxy, methyl, or hydroxyl group, respectively), and as a result, we predict that similar helical twists should be expected depending on the handedness of the hemiaminal ether stereocenter. It is also worthy of note that complex **7** adopts a conformation with the hydroxyl group pointing away from the pyridine rings (Figure 1c). The same is true for the methyl substituent in compounds **5** and **6**, which is oriented axially (or, in Canary's terminology, anti).[33,40] As a result, we postulate that substitution on the hydroxyl group (e.g., an alkoxy group) has a minimal effect on the helical twist. Hence, the dominant twist of **3** should be similar to that of the corresponding complex **7**. Taken together, we predict that the

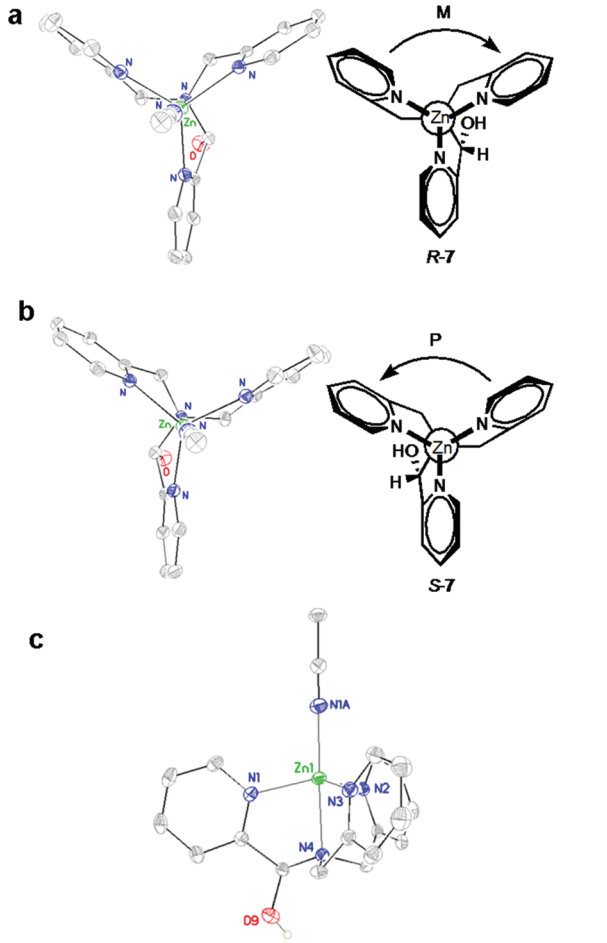

Figure 1. X-ray crystal structures of (a) *R*-**7** and (b) *S*-**7** with their corresponding Newman projections. The side view of the structure *S*-**7** is shown in (c). Displacement ellipsoids are scaled to the 50% probability level. The circles in the Newman projections represent the tertiary amine nitrogens.

isomers **3**(*S*, *R*), **3**(*R*, *S*), **3**(*R*, *R*), and **3**(*S*, *S*) would have a dominant *P*, *M*, *M*, and *P* helical twists, respectively.

Preferential Diastereomer. Having established a model to predict the dominant helical twist of the diastereomers of complex **3**, we next set out to create a model to predict the preference of the diastereomers induced by the chiral secondary alcohol. Nucleophilic attack on the *Re* and *Si* faces of **4** by an arbitrary R^1R^2CHOH was used to create a model (Scheme 4). To allow for facile visualization of possible steric interactions, the Newman projection of the *R* alcohol was drawn looking down the C–O bond [R^1 has a higher Cahn–Ingold–Prelog (CIP) priority[42] than R^2], and the OH was presumed to add from the Bürgi–Dunitz angle.[43] With the assumption that R^1 is bulkier than R^2, the bigger group (R^1) and smaller group (R^2) were placed to minimize steric hindrance. We postulate that the H on the stereocenter of the alcohol would preferentially be placed toward the pyridine group on the iminium carbon during nucleophilic addition, while both R^1 and R^2 would be placed near the H on the iminium carbon. If an *R* alcohol were to approach iminium **4** from the *Re* face (Scheme 4a), an *R* stereocenter would be generated, but disfavored steric interactions between R^1 and **4** would be expected. However, if an *R* alcohol were to attack **4** from the *Si* face (Scheme 4b), the steric hindrance between R^2 and **4** would be smaller with R^1

dx.doi.org/10.1021/ja301252h | J. Am. Chem. Soc. 2012, 134, 7117–7125

Scheme 4. Nucleophilic Addition of an *R* Alcohol to Iminium 4 (Py = 2-Pyridyl); the Newman Projection of the Alcohol Is Shown To Visualize the Steric Interactions

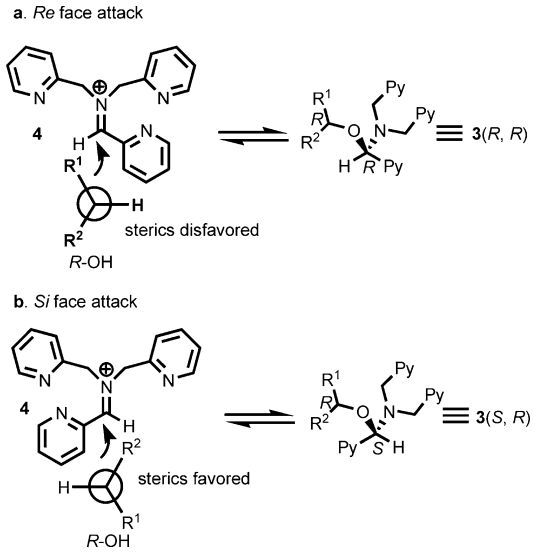

near the smaller H, hence predicting the preferential formation of an *S* stereocenter [i.e., **3**(*S*, *R*)]. Similarly, **3**(*R*, *S*) would be the major diastereomer if an *S* alcohol was used.

Computational Analysis. We now have two models. The first one correlates *R* and *S* hemiaminal ether stereochemistry to *M* and *P* helical twists, respectively. The second model predicts that *R* and *S* alcohols will preferentially create *S* and *R* hemiaminal ether stereocenters, respectively. As a result, we can tie *R* alcohols to *P* twists and *S* alcohols to *M* twists. However, Scheme 4 presents a steric-based model for kinetic analysis of nucleophilic attack geometries, while in a reversible reaction, the outcome is thermodynamically controlled. Hence, we simply postulated that the kinetic preference of chirality at the hemiaminal ether carbon correlates with the thermodynamic preference between the resulting diastereomers at equilibrium. To test this postulate, computational approaches were employed to predict diastereomeric ratios and the preferential twist on the basis of the configuration of the newly created stereocenter.

PEO was chosen for analysis, and the derived hemiaminal ether complex (**3-PEO**) was considered. The starting structures for molecular modeling were obtained from the X-ray geometry of compound **7**, and the four possible diastereomers of **3-PEO** derived from *S*-**PEO** were generated: *M*-(*R*, *S*), *P*-(*R*, *S*), *M*-(*S*, *S*), and *P*-(*S*, *S*). A chloride ion instead of an acetonitrile molecule was placed at the axial position. The coordination of chloride to the zinc center is supported by mass spectral analysis as well as the counterion effect.[38] For all of the isomers, multiple conformations were possible, including those with the ether group oriented axially (anti) or equatorially (syn). Preliminary conformational searches were run with molecular mechanics (MMFF), after which density functional theory (DFT) geometry optimizations were performed using the B3LYP functional and the 6-31G(d) basis set for all atoms. Relative zero-point-corrected (ZPC) free energies were evaluated by frequency calculations at the same level. The calculations revealed that the *M*-(*R*, *S*) diastereomer is by far the most stable one, accounting for about 90% of the Boltzmann population at 300 K (sum of two conformers, both with an axial ether group; the global minimum is shown in Figure 2a). The next most stable isomer is *P*-(*S*, *S*), constituting 8% of the population (sum of two conformers, both with an

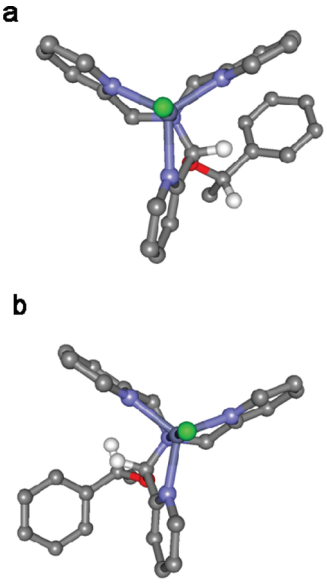

Figure 2. B3LYP/6-31G(d) lowest-energy structures for the **3**-*S*-**PEO** Zn complex (charge +1): (a) *M*-(*R*, *S*)-**3-PEO** (global minimum); (b) *P*-(*S*, *S*)-**3-PEO** (+1.49 kcal/mol). The green spheres represent Cl^-.

axial ether group; the minimum-energy structure is shown in the Figure 2b). The ZPC free energy difference between the more stable conformer of the *P*-(*S*, *S*) configuration and the global minimum of the *M*-(*R*, *S*) configuration was 1.49 kcal/mol. Other isomers, and in general conformations with equatorial ether groups, were negligible. The calculations confirmed and supported the predictions made above concerning a correlation between the kinetic and thermodynamic preferences at the newly formed stereocenter as well as the dominant helical twists, although the calculated *dr* for **PEO** at 300 K was larger than observed (9 vs 2.18).

CD Spectra. The chiral alcohols (Scheme 2) have small or no CD signals above 225 nm, and the other achiral substrates (Scheme 1) are CD-silent. As a result, any strong CD signals above 225 nm are indicative of complex **3** and in turn should correlate with the chirality of the alcohol. Before comparing the CD spectra of complex **3** derived from different alcohols, we set out to explore the alcohol concentration dependence to find the number of equivalents of a chiral alcohol that would lead to nearly level values of the CD ellipticity (i.e., saturation). In general, saturation affords the best signal-to-noise ratio, and the spectra will no longer be concentration-dependent. The assembly was conducted with varied concentrations of *R*- or *S*-**PEO** in the presence of activated 3 Å molecular sieves (35 mM **2-PA**, $Zn(OTf)_2$, and CEM-HCl, 42 mM **DPA**), and the CD spectra were recorded after dilution (0.175 mM total **2-PA**, 1 cm cell). The analogous multicomponent assembly reaction with 2-propanol has an equilibrium constant in the range of 10^8–10^9 M^{-2},[38] and hence, we expected that the assembly would be stable enough upon dilution for CD measurement. The CD spectra for *S*-**PEO** are shown in Figure 3a. Titration isotherms (Figure 3b) indicated that with 3–4 equiv of alcohol, the spectra are reasonably constant. Hence, all subsequent experiments were conducted using 3 equiv of alcohol.

The multicomponent assembly incorporating **PEO** led to large and reproducible CD signals (Figure 3), and ECCD was

dx.doi.org/10.1021/ja301252h | J. Am. Chem. Soc. 2012, 134, 7117–7125

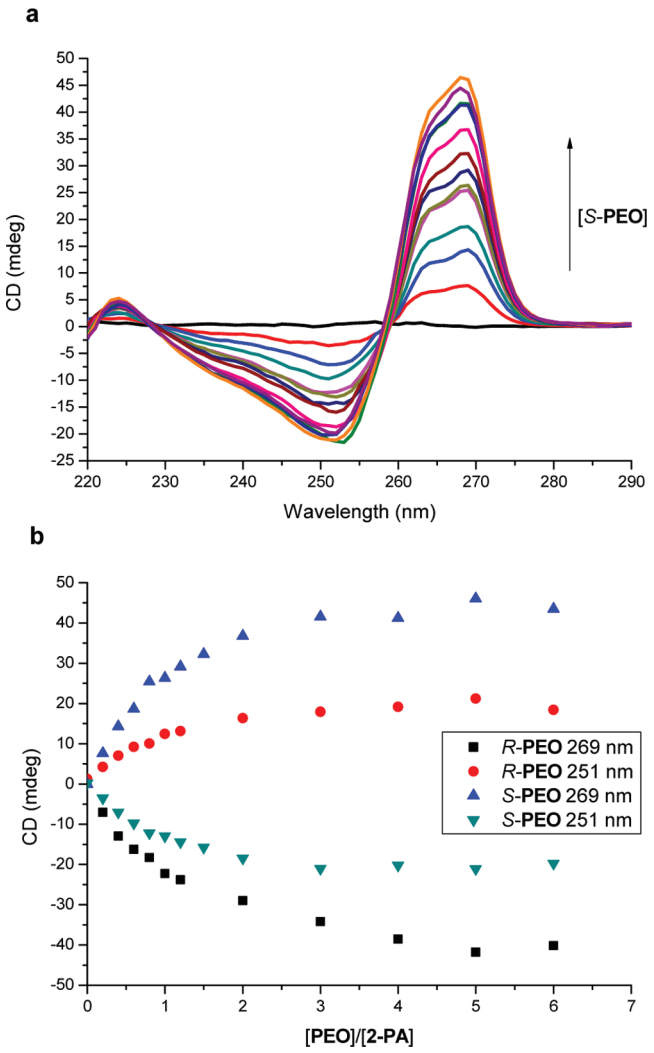

Figure 3. (a) CD spectra of the *S*-**PEO**-derived assembly at various alcohol concentrations. (b) CD intensity of assembly **3** at various concentrations of *R*- or *S*-**PEO**. The CD spectra were recorded in CH_3CN at 25 °C (0.175 mM **2-PA**, 1 cm cell).

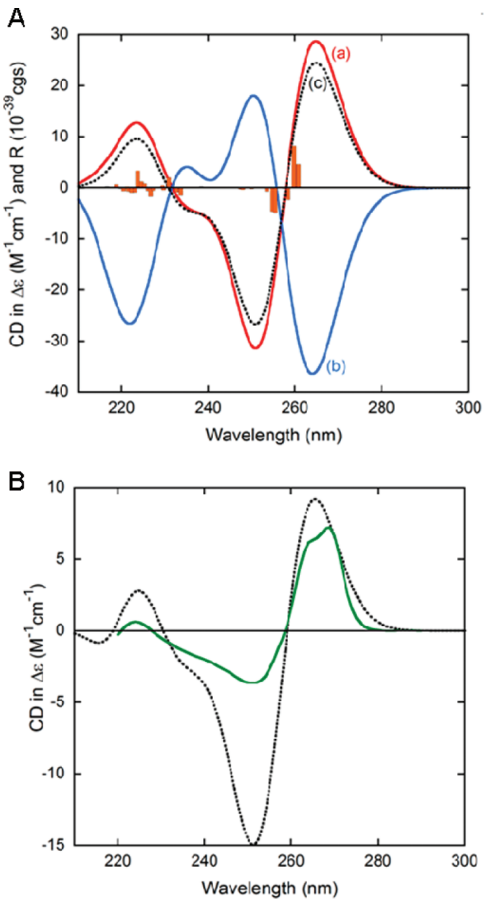

Figure 4. (A) CAM-B3LYP/SVP-calculated CD spectra for the **3**-*S*-**PEO** Zn complex (charge +1) for (a) the lowest-energy conformation of the *M*-(*R*, *S*) isomer (the vertical bars are the corresponding rotational strengths), (b) the lowest-energy conformation of the *P*-(*S*, *S*) isomer, and (c) the Boltzmann-weighted average (using ZPC free energies) for low-energy DFT-optimized structures. Gaussian exponential bandwidth, 0.225 eV; wavelength shift, +30 nm. (B) Comparison between the experimental CD spectrum of the **3**-*S*-**PEO** Zn complex (green) and the calculated spectrum estimated using the experimental diastereomeric ratio of 2.18 between the **3**(*R*, *S*) and **3**(*S*, *S*) isomers (black).

indicated by the fact that the null of the CD spectra is near the absorbance peak of the UV/vis spectra (see the Supporting Information). Two new peaks at 268 and 251 nm, respectively, were observed. *S*-**PEO** gave a positive first Cotton effect, while the *R* isomer gave an equal but opposite Cotton effect. The sign of the ECCD couplet was further explored using computation studies as described below.

Computational Modeling of the ECCD Spectra. CD calculations on the Zn complex **3**-**PEO** were run using time-dependent DFT (TDDFT)[44,45] to confirm the ECCD nature of the signals in the 230−280 nm region and to correlate the dominant structure of the complex with the CD profile. CD calculations were conducted in vacuo at the CAM-B3LYP/SVP level; other functionals (B3LYP) and larger basis sets (TZVP), as well as the inclusion of a solvent (PCM model for acetonitrile), did not substantially modify the results. Figure 4A reports the calculated CD spectra of *S*-**PEO**-derived assembly **3** for (a) the most stable *M*-(*R*, *S*) isomer of the **3**-*S*-**PEO** Zn complex in its lowest-energy conformation (shown in Figure 2a), (b) the lowest-energy conformation of the next most stable isomer *P*-(*S*, *S*) (shown in Figure 2b), and (c) the Boltzmann-weighted average (using ZPC free energies) for all of the DFT-optimized structures of the **3**-*S*-**PEO** Zn complex having populations larger than 1% at 300 K.

Inspection of Figure 4A demonstrates that the sign of the CD spectrum, in particular the couplet centered at 260 nm, is determined by the *M* or *P* helicity of the complex, with *M* helicity leading to a positive couplet and *P* helicity to a negative couplet. This is easily rationalized in terms of an ECCD picture.[46] In fact, orbital and population analysis clearly show that the most intense transitions calculated at ∼260 nm (see vertical bars in Figure 4) are ligand-centered $\pi-\pi^*$ transitions that are coupled with each other according to the exciton chirality theory. In particular, the involved transition is the $^1B_2$-type transition (also indicated as the B band) of the pyridine chromophore,[47] which is polarized perpendicular to the N−C4 direction. Phenyl-centered excitations participate to a very low extent in the transitions at ∼260 nm. For *M* helicity of the propeller, the exciton coupling of the three quasi-degenerate pyridine $^1B_2$-type transitions is expected to yield a positive ECCD couplet, as observed.[48] It is also clear that for *S*-**PEO**, the preference for the *R* configuration at the hemiaminal ether center, and in turn for a complex with *M* helicity, translates into

dx.doi.org/10.1021/ja301252h | *J. Am. Chem. Soc.* 2012, 134, 7117−7125

a positive couplet. In fact, the contribution of the dominant complex [the *M*-(*R*, *S*) isomer] also largely prevails in terms of the chiroptical response.

It was also worthwhile to calculate the CD spectrum using the experimental *dr* value. In Figure 4B, the experimental spectrum for *S*-**PEO**-derived assembly **3** is compared with the average of the spectra of the *M*-(*R*, *S*) and *P*-(*S*, *S*) diastereomers calculated using the experimental *dr* instead of the DFT-estimated one (2.18 rather than 9). It is apparent that the positions and signs of three Cotton effects (at 269, 252, and 224 nm) match very well. Moreover, the simulated CD magnitude at the first Cotton effect is in close agreement with the experimental data considering that 80−90% of *S*-**PEO**-derived assembly **3** is present at equilibrium by ^{1}H NMR studies. In summary, an *S* alcohol preferentially leads to complex **3**(*R*, *S*), which imparts an *M* twist to the pyridine, which then leads to a positive first Cotton effect.

Chirality Discrimination. We next set out to determine whether the preferential twist in the tris(pyridine) assembly would consistently predict the chirality. The CD spectra of the assembled complexes **3** derived from each enantiomer of several alcohols (Scheme 2) are shown in Figure 5. Although

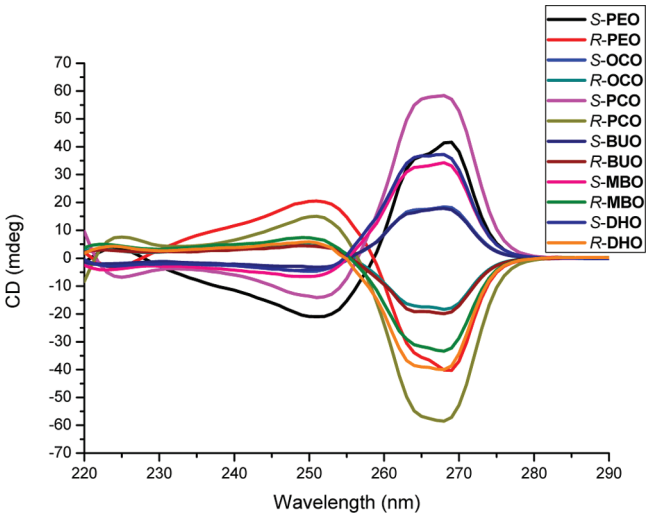

Figure 5. CD spectra of assemblies **3** derived from the alcohols in Scheme 2. The CD spectra were recorded in CH_3CN at 25 °C (0.175 mM **2-PA**, 1 cm cell).

each alcohol exhibited unique CD behavior, all of the *S* alcohols showed a positive first Cotton effect, while the corresponding *R* alcohols give CD spectra that were mirror images. Hence, the sign of the first Cotton effect can be employed to assign the absolute configuration of the stereocenter on the α-carbon: *R* stereocenters afford a negative signal and *S* stereocenters a positive signal at 268 nm.

In addition to changes in the CD magnitude at the two Cotton effects (for more details, see the companion paper, DOI 10.1021/ja3012534), the subtly different shapes of the CD curves between 230 and 275 nm must be dictated by the groups attached to the α-carbon of the alcohol. For example, the Cotton effect at 251 nm is more intense for the guests containing aromatic groups (**PEO** and **PCO**) than for those with aliphatic groups (**BUO**, **OCO**, **MBO**, and **DHO**). The variation of both the magnitude and shape of the CD curves paves the way for the possible discrimination of the identity of the alcohols via pattern recognition.

Pattern Recognition. To differentiate the identities of the alcohols, linear discriminant analysis (LDA) was applied to analyze the CD data.[49] LDA is a supervised pattern recognition protocol used for the classification of data as well as the assignment of new analytes to their appropriate classes. For a series of analytes, LDA creates functions based on the input data to minimize the distance of data points for a single analyte class and maximize the separation for different classes of analytes. For this purpose, each experiment was repeated five times using 3 equiv of each enantiomer of each alcohol to ensure reproducibility. The ellipticities at five wavelengths (238, 248, 258, 268, and 278 nm) were analyzed. These wavelengths were chosen to cover the full range of the CD spectra as well as the region where the signal varied the most. The resulting LDA plot is shown in Figure 6.

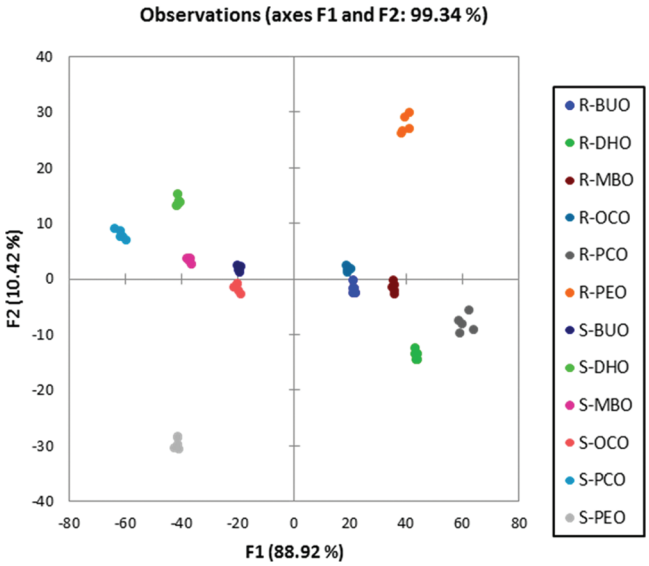

Figure 6. LDA plot for six enantiomeric pairs of chiral alcohols.

Excellent separation of the alcohol analytes was observed. The LDA plot shows 88.9% of the separation along the F1 axis and 10.4% along the F2 axis. The F1 axis discriminates the handedness of the chiral alcohols, with *S* alcohols on the left side and *R* alcohols on the right side. The enantiomers of each alcohol are reflected through the origin onto each other, confirming the mirror-image relationship of the CD spectra for *R*- and *S* alcohol-derived assemblies. The value on the F1 axis is in accordance with the intensity of the first Cotton effect at 268 nm, with **BUO** and **OCO** having the smallest absolute values and **PCO** the greatest.

The separation along F2 presumably reflects the magnitude at the second Cotton effect at 251 nm as well as the shape of the CD curve. This axis correlates with the chemical structure of the alcohol analyte. The three acyclic aliphatic alcohols have F2 values near 0, while the aryl alcohol **PEO** has the largest F2 value. The F2 values of the two cyclic alcohols are in the middle. The LDA classification via jack-knife analysis was 100%. Thus, both the chemical identity and handedness of secondary alcohol analytes can be successfully assigned.

Conformational Effects. After finding that the sign of the CD couplets is indicative of the chirality at the alcohol α-carbon and that the magnitude of the CD spectrum varies with the alcohol, we set out to examine further the effect of alcohol structure on the CD spectrum by expanding the scope of the

alcohol analytes. Six heteroatom-containing alcohols, including both acyclic and cyclic ones, were chosen (Scheme 5): *R*-1-benzyloxy-2-propanol [*R*-**BPO**], *S*-1-benzyloxy-2-propanol [*S*-**BPO**], *R*-1-methoxy-2-propanol (**OPO**), *R*-1-benzyl-3-hydroxypyrrolidine (**BHP**), *S*-1-methyl-3-hydroxypyrrolidine (**MHP**), and *S*-3-hydroxytetrahydrofuran (**HHF**). The *dr* values for **BPO**- and **OPO**-derived assemblies **3** are 1.43 and 1.29, respectively, while those of assemblies **3** derived from **BHP**, **MHP**, and **HHF** are similar (~1.2).

Scheme 5. Structures of Heteroatom-Containing Chiral Secondary Alcohols

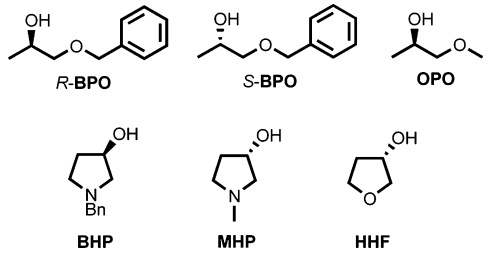

The CD spectra recorded for assemblies **3** derived from the heteroatom-containing alcohols are shown in Figure 7. The *R*

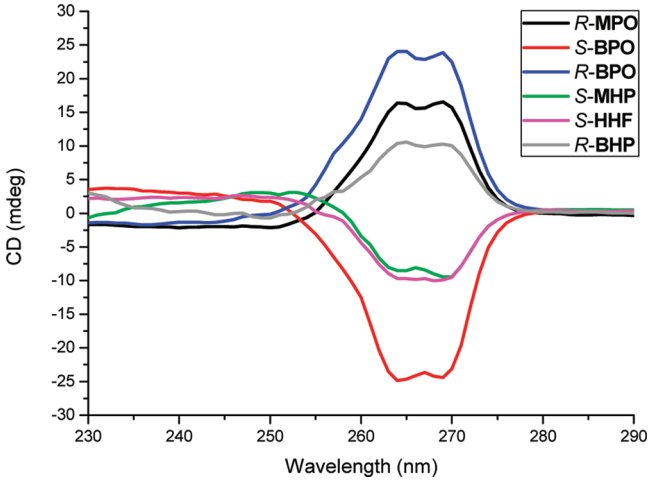

Figure 7. CD spectra of the multicomponent assemblies derived from the alcohols in Scheme 5. The CD spectra were recorded in CH_3CN at 25 °C (0.175 mM **2**-**PA**, 1 cm cell).

alcohols gave a positive Cotton effect and the *S* alcohols afforded a negative one at 268 nm, which is opposite to the results for the alcohols listed in Scheme 2. The striking difference between the CD spectra for the alcohols in Schemes 2 and 5 led us to explore how other factors, such as conformational effects imparted by the heteroatoms, would lead to differences in the *M* and *P* twists of the pyridines.

The Cotton effect reversal that was the simplest to explain derives from a nomenclature issue. For the two pyrrolidine-based alcohols in Scheme 5 (**BHP** and **MHP**), the major conformer adopts a trans configuration for 3-OH and the substituent on the nitrogen to avoid the disfavorable steric interactions (Scheme 6a). As a result, position 5 is bulkier than position 1 (H over an electron lone pair) even though position 1 has a higher CIP priority than position 5 (N over C), and therefore, the relationship between the sign of the Cotton effect and the alcohol's stereochemistry nomenclature is reversed. A

Scheme 6. (a) Trans Isomer of *R*-BHP; (b) Comparison of the Conformer Distributions of *R*-BUO and *R*-OPO (DFT-Estimated Populations at 300K); (c) Additional Stabilizing Effect in the Favorable Gauche Rotamer of *R*-OPO (L = Other Ligands on Zinc)

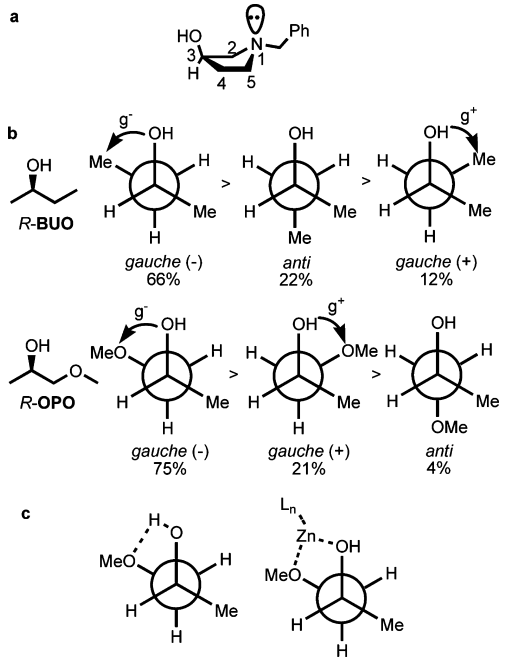

similar argument can be made for oxygen-containing **HHF**. The preferential trans conformation of these cyclic alcohols is postulated to be maintained from the alcohol substrate to the final assembled complex. In addition to the effect on the sign of the CD couplet, another consequence is that the heteroatom and substitution on it would have a minimal effect on the *dr* values and CD magnitude, which is supported by the similar *dr* values (~1.2) and absolute values of CD intensities at 268 nm (~10 mdeg) for *R*-**BHP**, *S*-**MHP**, and *S*-**HHF**.

Insights can be obtained for the acyclic alcohols in Scheme 5 by conformational analysis. To visualize the steric interactions, Newman projections of *R*-**BUO** and *R*-**OPO** were drawn looking down the bond from the α carbon to the β carbon, and only the staggered conformers are shown (Scheme 6b). These two alcohols were chosen because the only difference between them is the substituent on the β carbon (methyl or methoxy, respectively). Conformational distributions were calculated using DFT (at B3LYP/6-31G(d) level in vacuo; populations at 300K estimated from internal energies are shown in Scheme 6b). For *R*-**BUO**, the two bulkier methyl groups were found to be preferentially oriented anti to each other, as may be expected. Hence, the methyl on the β carbon is gauche to the hydroxyl (i.e., the g^- conformer). The other gauche isomer (g^+) has the smallest distribution, while the anti conformer is in the middle.

A similar preferred gauche (−) conformer was found for *R*-**OPO** on the basis of DFT conformational analysis (Figure 6b). In this g^- conformer, the hydroxyl and methoxy were placed gauche to each other, and the methyl on the α carbon is anti to the methoxy. However, in contrast to *R*-**BUO**, the anti rotamer has the smallest distribution while the g^+ rotamer is in the middle. Such gauche rotamers are preferred because of the so-called "gauche effect".[50,51] More importantly, intramolecular hydrogen-bond- or zinc-mediated chelation (Scheme 6c) can

dx.doi.org/10.1021/ja301252h | *J. Am. Chem. Soc.* 2012, 134, 7117−7125

lead to further stabilization of the gauche conformers. In either scenario, a five-membered ring would form, and CH_2O would become part of the ring skeleton.

To explain the stereochemistry at the newly formed stereocenter, our model placed substituents on *R*-**OPO** to minimize steric interactions with iminium **4** (Scheme S1 in the Supporting Information). If *R*-**OPO** were to attack **4** from the *Si* face, disfavored steric interactions between the α-methyl and pyridine would exist. In contrast, we postulate that if *R*-**OPO** were to approach **4** from the *Re* face, the α-methyl and α-H on *R*-**OPO** would be best placed toward the iminium H and pyridine on **4**, respectively, as a result of more favorable steric interactions (see Scheme S1). This is opposite to Scheme 4, where attack at the *Si* face dominates. As a result, *R*-**OPO** leads to a reversal of the preferential stereochemistry of the hemiaminal ether carbon and thereby the sign of the CD couplet. A similar argument can be made for **BPO**. It is worthwhile to note that the reversal of stereoselectivity mediated by chelate control is not uncommon in organic chemistry.[52]

Calibration of *ee* and Analysis. After discriminating both the chiralities and identities of the alcohol analytes, we moved forward to *ee* measurements on unknowns. For this purpose, *ee* calibration curves were generated. **PEO**, **OCO**, and **PCO** were chosen because they represent three types of structures (aromatic, aliphatic, and cyclic, respectively) and cover a wide range of CD magnitudes. The assembly reactions were conducted using 3 equiv of alcohol to ensure that the signal was saturated. To ensure reproducibility, the *ee* calibration curves were constructed using data at 11 *ee* values (−100, −80, −60, −40, −20, 0, 20, 40, 60, 80, and 100%), with each point being an average of three independent measurements.

For example, the CD spectra for **PCO** at various *ee*'s are shown in Figure 8a, and the reproducibility of the data for both peaks (251 and 268 nm) was excellent (Figure 8b). All three alcohols gave linear calibration lines with R^2 near 0.99 (see the Supporting Information). The CD spectra of at least 12 unknown samples of varying *ee* for each alcohol were recorded, and the corresponding calibration curves were used to calculate the *ee*'s (Table S1 in the Supporting Information). The average absolute errors were 2.3, 2.4, and 2.6% for **PEO**, **OCO**, and **PCO**, respectively. Such accuracy is high for an optical *ee* assay, and the error of ~3% falls well within the threshold of error needed for the screening of asymmetric catalysts and reactions.[10]

SUMMARY

A sensing ensemble built from a dynamic covalent multicomponent assembly reaction has been employed to explore the handedness of chiral secondary alcohols using ECCD. The ECCD, which results from a helical twist in the tris(pyridine) zinc complex induced by the chiral mono-ol, was rationalized by qualitative chemical models as well as computational studies. The absolute configurations of the chiral alcohols were successfully determined by the positive or negative signs of Cotton effects, while the identities of the alcohols were unambiguously discriminated by the magnitudes as well as the shapes of the CD spectra using linear discriminant analysis. Conformational effects induced by heteroatoms were also explored to expand further the scope of alcohol analytes. Lastly, *ee* calibration curves were constructed for three representative alcohols, and the *ee*'s of test samples were determined with an average error of less than 3%. Current efforts are focused on transitioning the assays described here to asymmetric reaction screening.

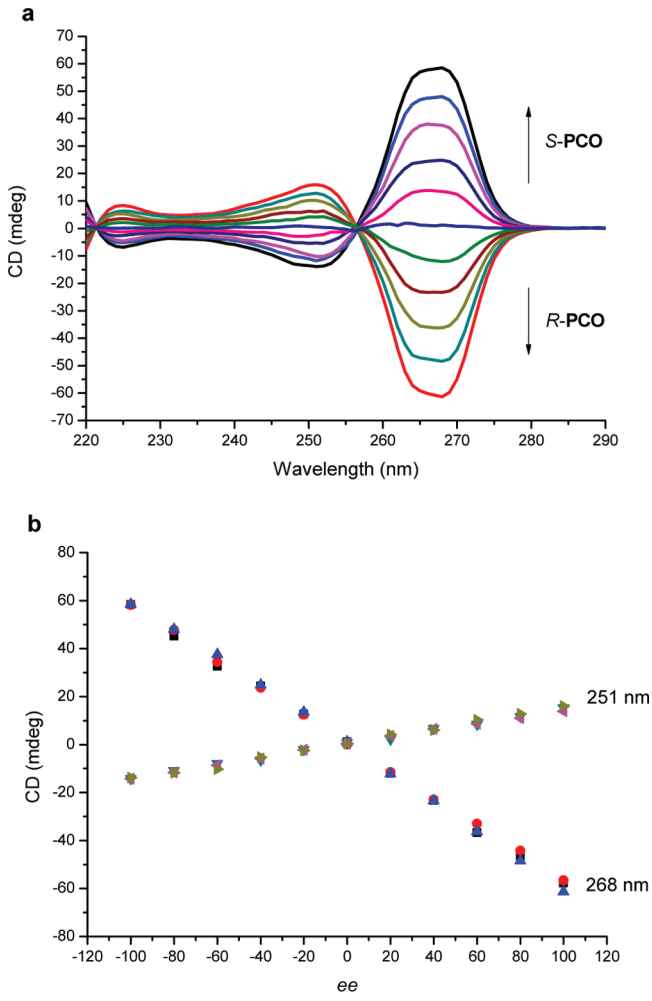

Figure 8. (a) CD spectra for the assemblies derived from **PCO** with different *ee*'s. The CD spectra were recorded in CH_3CN at 25 °C (0.175 mM **2-PA**, 1 cm cell). (b) Corresponding calibration curves for **PCO** at 251 and 268 nm (for experimental details, see the Supporting Information).

ASSOCIATED CONTENT

Supporting Information

Experimental details, spectra data, *ee* calibration lines, and unknown *ee* calculations. This material is available free of charge via the Internet at http://pubs.acs.org.

AUTHOR INFORMATION

Corresponding Author

anslyn@austin.utexas.edu; ldb@dcci.unipi.it

Notes

The authors declare no competing financial interest.

ACKNOWLEDGMENTS

We thank the National Institute of Heath (GM 77437) and the Welch Foundation (F-1151) for financial support. We thank Dr. Ryota Saito for helpful discussions.

REFERENCES

(1) Denmark, S. E.; Fu, J. *Chem. Rev.* **2003**, *103*, 2763−2794.

(2) Walsh, P. J. *Acc. Chem. Res.* **2003**, *36*, 739−749.
(3) Ikariya, T.; Blacker, A. J. *Acc. Chem. Res.* **2007**, *40*, 1300−1308.
(4) Skucas, E.; Ngai, M. Y.; Komanduri, V.; Krische, M. J. *Acc. Chem. Res.* **2007**, *40*, 1394−1401.
(5) Han, S. B.; Han, H.; Krische, M. J. *J. Am. Chem. Soc.* **2010**, *132*, 1760−1761.
(6) Reetz, M. T. *Angew. Chem., Int. Ed.* **2001**, *40*, 284−310.
(7) Joyce, L. A.; Shabbir, S. H.; Anslyn, E. V. *Chem. Soc. Rev.* **2010**, *39*, 3621−3632.
(8) Schurig, V. *J. Chromatogr., A* **2001**, *906*, 275−299.
(9) Welch, C. J.; Hyun, M. H.; Kubota, T.; Schafer, W.; Bernardoni, F.; Choi, H. J.; Wu, N.; Gong, X.; Lipshutz, B. *Chirality* **2008**, *20*, 815−819.
(10) Leung, D.; Kang, S. O.; Anslyn, E. V. *Chem. Soc. Rev.* **2012**, *41*, 448−479.
(11) Zhu, L.; Zhong, Z.; Anslyn, E. V. *J. Am. Chem. Soc.* **2005**, *127*, 4260−4269.
(12) Leung, D.; Folmer-Andersen, J. F.; Lynch, V. M.; Anslyn, E. V. *J. Am. Chem. Soc.* **2008**, *130*, 12318−12327.
(13) Shabbir, S. H.; Joyce, L. A.; da Cruz, G. M.; Lynch, V. M.; Sorey, S.; Anslyn, E. V. *J. Am. Chem. Soc.* **2009**, *131*, 13125−13131.
(14) Pu, L. *Chem. Rev.* **2004**, *104*, 1687−1716.
(15) Hembury, G. A.; Borovkov, V. V.; Inoue, Y. *Chem. Rev.* **2008**, *108*, 1−73.
(16) Nieto, S.; Lynch, V. M.; Anslyn, E. V.; Kim, H.; Chin, J. *J. Am. Chem. Soc.* **2008**, *130*, 9232−9233.
(17) Nieto, S.; Dragna, J. M.; Anslyn, E. V. *Chem.—Eur. J.* **2010**, *16*, 227−232.
(18) Leung, D.; Anslyn, E. V. *Org. Lett.* **2011**, *13*, 2298−2301.
(19) Berova, N.; Di Bari, L.; Pescitelli, G. *Chem. Soc. Rev.* **2007**, *36*, 914−931.
(20) Borovkov, V. V.; Lintuluoto, J. M.; Inoue, Y. *J. Am. Chem. Soc.* **2001**, *123*, 2979−2989.
(21) Borovkov, V. V.; Lintuluoto, J. M.; Inoue, Y. *Org. Lett.* **2000**, *2*, 1565−1568.
(22) Kim, H.; So, S. M.; Yen, C. P.; Vinhato, E.; Lough, A. J.; Hong, J. I.; Kim, H. J.; Chin, J. *Angew. Chem., Int. Ed.* **2008**, *47*, 8657−8660.
(23) Huang, X.; Fujioka, N.; Pescitelli, G.; Koehn, F. E.; Williamson, R. T.; Nakanishi, K.; Berova, N. *J. Am. Chem. Soc.* **2002**, *124*, 10320−10335.
(24) Iwaniuk, D. P.; Wolf, C. *J. Am. Chem. Soc.* **2011**, *133*, 2414−2417.
(25) Iwaniuk, D. P.; Wolf, C. *Org. Lett.* **2011**, *13*, 2602−2605.
(26) Ghosn, M. W.; Wolf, C. *J. Am. Chem. Soc.* **2009**, *131*, 16360−16361.
(27) Li, X.; Tanasova, M.; Vasileiou, C.; Borhan, B. *J. Am. Chem. Soc.* **2008**, *130*, 1885−1893.
(28) Li, X.; Borhan, B. *J. Am. Chem. Soc.* **2008**, *130*, 16126−16127.
(29) Kurtan, T.; Nesnas, N.; Li, Y. Q.; Huang, X.; Nakanishi, K.; Berova, N. *J. Am. Chem. Soc.* **2001**, *123*, 5962−5973.
(30) Kurtan, T.; Nesnas, N.; Koehn, F. E.; Li, Y. Q.; Nakanishi, K.; Berova, N. *J. Am. Chem. Soc.* **2001**, *123*, 5974−5982.
(31) Lintuluoto, J. M.; Borovkov, V. V.; Inoue, Y. *J. Am. Chem. Soc.* **2002**, *124*, 13676−13677.
(32) Zahn, S.; Canary, J. W. *Org. Lett.* **1999**, *1*, 861−864.
(33) Castagnetto, J. M.; Xu, X.; Berova, N. D.; Canary, J. W. *Chirality* **1997**, *9*, 616−622.
(34) Holmes, A. E.; Zahn, S.; Canary, J. W. *Chirality* **2002**, *14*, 471−477.
(35) Zhang, J.; Holmes, A. E.; Sharma, A.; Brooks, N. R.; Rarig, R. S.; Zubieta, J.; Canary, J. W. *Chirality* **2003**, *15*, 180−189.
(36) Holmes, A. E.; Das, D.; Canary, J. W. *J. Am. Chem. Soc.* **2007**, *129*, 1506−1507.
(37) Joyce, L. A.; Maynor, M. S.; Dragna, J. M.; da Cruz, G. M.; Lynch, V. M.; Canary, J. W.; Anslyn, E. V. *J. Am. Chem. Soc.* **2011**, *133*, 13746−13752.
(38) You, L.; Berman, J. S.; Anslyn, E. V. *Nat. Chem.* **2011**, *3*, 934−938.
(39) Anslyn, E. V.; Dougherty, D. A. *Modern Physical Organic Chemistry*; University Science Books: Sausalito, CA, 2006.
(40) Canary, J. W.; Allen, C. S.; Castagnetto, J. M.; Chiu, Y.-H.; Toscano, P. J.; Wang, Y. *Inorg. Chem.* **1998**, *37*, 6255−6262.
(41) You, L.; Long, S. R.; Lynch, V. M.; Anslyn, E. V. *Chem.—Eur. J.* **2011**, *17*, 11017−11023.
(42) Cahn, R. S.; Ingold, C.; Prelog, V. *Angew. Chem., Int. Ed. Engl.* **1966**, *5*, 385−415.
(43) Bürgi, H. B.; Dunitz, J. D.; Lehn, J. M.; Wipff, G. *Tetrahedron* **1974**, *30*, 1563−1572.
(44) Autschbach, J.; Nitsch-Velasquez, L.; Rudolph, M. *Top. Curr. Chem.* **2011**, *298*, 1−98.
(45) Di Bari, L.; Pescitelli, G. Electronic Circular Dichroism. In *Computational Spectroscopy: Methods, Experiments and Applications*; Grunenberg, J., Ed.; Wiley-VCH: Weinheim, Germany, 2010; pp 241−277.
(46) Harada, N.; Nakanishi, K. *Circular Dichroic Spectroscopy: Exciton Coupling in Organic Stereochemistry*; University Science Books: Mill Valley, CA, 1983.
(47) Jaffé, H. H.; Orchin, M. *Theory and Application of Ultraviolet Spectroscopy*; Wiley: New York, 1962.
(48) Fan, J.; Ziegler, T. *Chirality* **2011**, *23*, 155−166.
(49) Johnson, R. A.; Wilchern, D. W. *Applied Multivariate Statistical Analysis*; Prentice-Hall: Englewood Cliffs, NJ, 1982.
(50) Craig, N. C.; Chen, A.; Suh, K. H.; Klee, S.; Mellau, G. C.; Winnewisser, B. P.; Winnewisser, M. *J. Am. Chem. Soc.* **1997**, *119*, 4789−4790.
(51) Goodman, L.; Gu, H.; Pophristic, V. *J. Phys. Chem. A* **2005**, *109*, 1223−1229.
(52) Mengel, A.; Reiser, O. *Chem. Rev.* **1999**, *99*, 1191−1223.